

Unusual electrical and magnetic properties in layered EuZn_2As_2

Joanna Blawat^{1,2}, Madalynn Marshall³, John Singleton⁴, Erxi Feng⁵, Huibo Cao⁵, Weiwei Xie³,
Rongying Jin^{1,*}

¹Center for Experimental Nanoscale Physics, Department of Physics & Astronomy, University of South Carolina, Columbia, SC 29208, USA

²Department of Physics & Astronomy, Louisiana State University, Baton Rouge, LA 70803, USA

³Department of Chemistry and Chemical Biology, Rutgers University, Piscataway, NJ 08854, USA

⁴National High Magnetic Field Laboratory, Los Alamos National Laboratory, Los Alamos, New Mexico 87545, USA

⁵Neutron Scattering Division, Oak Ridge National Laboratory, Oak Ridge, TN 37831, USA

Abstract

Eu-based compounds often exhibit unusual magnetism, which is critical for nontrivial topological properties seen in materials such as EuCd_2As_2 . We investigate the structure and physical properties of EuZn_2As_2 through measurements of the electrical resistivity, Hall effect, magnetization, and neutron diffraction. Our data show that EuZn_2As_2 orders antiferromagnetically with an A-type spin configuration below $T_N = 19$ K. Surprisingly, there is strong evidence for dominant ferromagnetic fluctuations above T_N , as reflected by positive Curie-Weiss temperature and extremely large negative magnetoresistance (MR) between T_N and $T_{\text{fl}} \approx 200$ K. Furthermore, the angle dependence of the MR_{ab} indicates field-induced spin reorientation from the ab -plane to a direction approximately 45° from the ab plane. Compared to EuCd_2As_2 , the doubled T_N and T_{fl} make EuZn_2As_2 a better platform for exploring topological properties in both magnetic fluctuation ($T_N < T < T_{\text{fl}}$) and ordered ($T < T_N$) regimes.

Key words: antiferromagnetic order, ferromagnetic fluctuations, type-IV magnetic space group, topological states

1. Introduction

Since the discovery of topological states in semimetals ^[1–6], the search for new topological materials has been extremely active. Time-reversal symmetry (\mathcal{T}) and crystal inversion symmetry (\mathcal{P}), together with the Kramers theorem (each energy band is doubly degenerate for fermions), are crucial in understanding the formation of topological states in semimetals^[1]. When both \mathcal{T} and \mathcal{P} are preserved, a system may host Dirac fermions at the Dirac points (DP), at which bands are quadruply degenerate. Several Dirac semimetals have been identified, including Cd_3As_2 ^[2], Na_3Bi ^[3], and ZrTe_5 ^[4]. When \mathcal{T} is broken but \mathcal{P} is preserved, one may expect two Weyl cones with opposite chirality in a Weyl semimetal. Considering the opposite situation, *i.e.*, \mathcal{T} is preserved but \mathcal{P} is broken, the number of Weyl cones is multiplied by four, removing the chirality^[1]. Weyl states have been observed in semimetals such as MoTe_2 ^[5,6], TaAs ^[7], WTe_2 ^[8], and TaIrTe_4 ^[9]. Breaking both \mathcal{T} and \mathcal{P} would generally destroy the Dirac/Weyl properties in these systems. An exception is that the Dirac state can exist if the symmetry of the product \mathcal{PT} is preserved [19]. A case study was carried out in magnetic CuMnAs , which belongs to a type-III magnetic space group with a C-

type spin structure ^[10,11]. Magnetic materials offer a fertile ground for searching for novel topological properties protected by the \mathcal{PT} symmetry.

Recently, materials with the type-IV magnetic space group have also been studied ^[12]. The type-IV magnetic space group is defined by $G + \mathcal{T}\{e|\tau\}G$, where G is the ordinary nonmagnetic space group, e is the identity operation and $\{e|\tau\}$ represents the translation operation between spin-up and spin-down sublattices in a magnetic space group ^[12]. In such a magnetic space group, there is a nonsymmorphic time-reversal \mathcal{T}' symmetry, which is related to \mathcal{T} through the translation operation τ ($\mathcal{T}' = \mathcal{T}\tau$). In the centrosymmetric type-IV magnetic space group, the symmetry of the product \mathcal{PT}' is preserved; therefore Kramers degeneracy is protected, and Dirac Points can exist ^[12]. EuCd_2As_2 has been theoretically predicted to be an antiferromagnetic (AFM) Dirac semimetal, in which DPs are protected by the \mathcal{PT}' symmetry ^[12]. EuCd_2As_2 forms an A-type AFM state below $T_N = 9.5$ K in which the threefold symmetry in the ab -plane is broken due to the spin configuration. According to theoretical calculations, this leads to a gap between Dirac cones^[13,14]. However, strong ferromagnetic (FM) fluctuations above T_N break the \mathcal{T} symmetry, giving rise to a Weyl state at high temperatures ($T > T_N$) ^[15]. Thus, such a system provides a rare case for studying the transition between the Dirac and Weyl states by tuning temperature. To further study the influence of magnetism on the topology of the electronic band structure, we investigate the physical properties of EuZn_2As_2 , a sister compound of EuCd_2As_2 . The replacement of Cd by Zn is expected to weaken the spin-orbit coupling, thus influencing the gap size between Dirac cones. In addition, compared to EuCd_2As_2 , we find that the AFM ordering temperature for EuZn_2As_2 , $T_N = 19$ K, is doubled, offering a much wider temperature range for studying potential topological properties in a long-range AFM ordered state. By analyzing magnetization and magneto-transport data, we also find strong evidence for ferromagnetic (FM) fluctuations over a much wider temperature range than that in EuCd_2As_2 . Such information is key toward the understanding of magnetism-driven topological properties.

2. Experimental methods

The single crystals of EuZn_2As_2 were grown via the flux method using Sn. The elemental Eu (99.9% pieces, Alfa Aesar), Zn (99.8% granules, Alfa Aesar), As (99.999% powder, Alfa Aesar) and Sn (99.9% granules, Alfa Aesar) were placed into an alumina crucible with a molar ratio $\text{Eu} : \text{Zn} : \text{As} : \text{Sn} = 1 : 2 : 2 : 20$, and sealed in an evacuated quartz tube. The sample was heated up to 600 °C at a rate of 60 °C/h, and kept at this temperature for 5 hours. This was followed warming

to 1000 °C and tempering for 10 hours. The sample was then slowly cooled (-3 °C/h) down to 600 °C with a further centrifuge in order to remove Sn flux. The resulting single crystals have a typical size of 4 mm × 2 mm × 1 mm and are stable in air.

The crystal structure was determined by single crystal X-ray diffraction using a Bruker Apex II single X-ray diffractometer equipped with Mo radiation ($\lambda_{K\alpha} = 0.71073 \text{ \AA}$), and by powder X-ray diffraction (PXRD) by means of a Rigaku MiniFlex 600 diffractometer with Cu $K_{\alpha 1}$ radiation ($\lambda = 1.5406 \text{ \AA}$). The crystal structure was solved with the full-matrix least-squares method using the SHELXTL package^[16]. The PXRD pattern was analyzed using the FullProf software^[17]. The crystal structure is drawn by means of VESTA software^[18].

The magnetic properties have been measured in a *Quantum Design* Magnetic Properties Measurement System (MPMS – 7 T). The electrical resistivity, Hall effect, and heat capacity were measured using a *Quantum Design* Physical Property Measurement System (PPMS – 14 T). The standard four-probe technique was used to measure the electrical resistivity and Hall effect, and the relaxation method used for the heat capacity. The angle dependence of the magnetoresistance (MR) was measured at the pulsed-field facility of National High Magnetic Field Laboratory (NHMFL, Los Alamos).

To determine the magnetic structure of EuZn_2As_2 , single-crystal neutron diffraction experiment was performed on DEMAND (HB-3A) at the High Flux Isotope Reactor (HFIR) of Oak Ridge National Laboratory (ORNL)^[19]. A wavelength of 1.008 Å from the bent Si-331 monochromator was used to reduce the heavy neutron absorption. Considering the large neutron absorption coefficient of Eu, PLATON software was employed to apply an absorption correction^[20,21]. The magnetic and nuclear structures were both determined using Fullprof refinement Suite software^[17].

3. Results and Discussion

The single crystal X-ray diffraction refinement confirms that our crystals form a trigonal structure with the formula EuZn_2As_2 . The space group is $P-3m1$ (No. 164) with the lattice parameters $a = b = 4.2093(1) \text{ \AA}$ and $c = 7.175(3) \text{ \AA}$. Replacing Cd with smaller Zn, the lattice parameters in EuZn_2As_2 decrease more significantly along the a and b axes ($\approx 5.5\%$ reduction) than the c axis ($\approx 2.4\%$ reduction). Detailed information including atomic positions and sites occupancies is summarized in Tables I and II. Figure 1(a) illustrates the crystal structure of

EuZn₂As₂, where Zn (green) and As (grey) form a honeycomb network separated by Eu atoms (pink). Figure 1(b) shows the X-ray diffraction pattern of a flat surface of a EuZn₂As₂ single crystal at room temperature. All peaks can be indexed with the above-mentioned structure from the (001) plane (i.e., the *ab*-plane). A weak peak near $2\theta \approx 30^\circ$ results from residual Sn on the surface. A picture of a EuZn₂As₂ single crystal is presented in the inset of Figure 1(b). The PXR pattern obtained from ground crystals was analyzed using the LeBail method and the result is presented in Figure S1. The red points, black and blue lines represent the experimentally observed intensities, calculated intensities, and the difference between them, respectively. The expected Bragg positions for EuZn₂As₂ are shown as green vertical marks. The LeBail analysis confirms that EuZn₂As₂ crystallizes in the above-mentioned trigonal crystal structure.

Figure 2(a) shows the temperature dependence of the zero-field-cooled (ZFC) and field-cooled (FC) magnetic susceptibility measured by applying a magnetic field of 0.1 T parallel to the *c*-axis (χ_c) and to the *ab*-plane (χ_{ab}), respectively. With decreasing temperature, both χ_{ab} and χ_c initially increase with little difference between them. Below $T_N = 19$ K, χ_{ab} tends to saturate but χ_c decreases. Such behavior implies that the system forms an A-type AFM order, with FM alignment in the *ab*-plane, but with an AFM configuration along the *c*-axis. The much higher T_N suggests stronger magnetic interactions both within the *ab* plane and along the *c* axis in EuZn₂As₂ than those in EuCd₂As₂^[22], consistent with the lattice parameter changes mentioned above.

To understand magnetic interactions in EuZn₂As₂, we fit χ_{ab} and χ_c between 100 K and 300 K using the Curie-Weiss formula $\chi(T) = C/(T - \theta)$, where θ is the Curie-Weiss temperature and C is the Curie constant related to the effective magnetic moment $\mu_{\text{eff}} = \sqrt{8C}$. As shown in the inset of Figure 2(a), the formula fits the data well (the solid lines are fitting curves). The parameters obtained are $\theta_{ab} = 48.3(6)$ K and $\mu_{\text{eff}}^{\text{ab}} = 7.08(5)$ μ_B , and $\theta_c = 25.1(2)$ K and $\mu_{\text{eff}}^c = 7.86(3)$ μ_B . The positive values of θ_{ab} and θ_c imply dominant ferromagnetic interactions between Eu ions, with the effective magnetic moment close to the theoretical value for Eu²⁺ ($\mu_{\text{eff}} = 7.94\mu_B$). Taking this at face value, one would expect there to be a difference between the magnetic susceptibility measured under zero-field-cooled (ZFC) and field-cooled (FC) modes; however, this is not seen (Figure 2(a)). Furthermore, the application of higher magnetic field should enhance the FM interactions. Figures 2(b) and 2(c) show the temperature dependences of χ_{ab} and χ_c between 2 and 60 K in various fields. Note that increased magnetic field pushes T_N to lower temperatures (Figure 2(d)).

Both observations indicate that EuZn_2As_2 is *not* a ferromagnet below T_N . As shown in Figure 2(e), the field dependence of the magnetization has no hysteresis in either M_{ab} or M_c at 2 K. Instead, both $M_{ab}(H)$ and $M_c(H)$ vary linearly with field before reaching saturation. The observed saturation moment is close to the theoretical value for Eu^{2+} ($\mu_{\text{sat}} = gJ = 7\mu_B$, where J is the total angular momentum and g is the Landé g factor)^[23].

To confirm the nature of the phase transition at T_N , we have measured the temperature and field dependence of the specific heat, C_p . Figure 2(f) shows the temperature dependence of C_p at $\mu_0H = 0$ and 9 T. Note that there is a lambda-shaped anomaly in $C_p(H = 0)$ at $T_N = 19$ K, indicating a second-order phase transition. The entropy released at the phase transition between 10 and 25 K is $S \approx 10.8 \text{ J mol}^{-1} \text{ K}^{-1}$, about 62.5% of the theoretically expected value for an 8-fold degenerate system [$S = R \ln(2J+1) = R \ln 8 = 17.28 \text{ J mol}^{-1} \text{ K}^{-1}$]. This reduced entropy is likely related to magnetic fluctuations, which release some amount of entropy above T_N . By applying $\mu_0H = 9$ T, the specific heat peak is completely suppressed. Notably, $C_p(\mu_0H = 9 \text{ T}) > C_p(H = 0)$ above 19 K, confirming partial entropy removal for the case of $H = 0$ prior to T_N .

Given the unusual magnetic behavior seen in the magnetization above and below T_N , it is essential to determine the magnetic structure of EuZn_2As_2 through single-crystal neutron diffraction experiment. Figure 3(a) shows the rocking curve scan at $(0 \ 0 \ \frac{1}{2})$ peak position at 4 K and 40 K. The peak disappears above T_N , indicating a magnetic propagation vector $\mathbf{k} = (0 \ 0 \ \frac{1}{2})$ for the ordered state. We find that the magnetic peaks collected at 4 K can be fit by an A-type magnetic structure with the magnetic moments entirely in the ab -plane within the data resolution. The resultant magnetic structure at 4 K is presented in Figure 3(b), which is ferromagnetically aligned in the ab plane but antiferromagnetic along the c axis. This A-type AFM structure is the same as those seen in EuCd_2As_2 grown with Sn flux^[14,22] and in EuMg_2Bi_2 ^[24] but different from that in EuIn_2As_2 ^[25]. At 4 K, the refined magnetic moment is $7.33(7)\mu_B/\text{Eu}$, slightly higher than the saturation value from the magnetization (Figure 2(e)). We choose the reflection intensity (I) at $(0 \ 0 \ \frac{1}{2})$ as the order parameter. The temperature dependence of I is shown in Figure 3(c). The solid curve is the fit of $I(T)$ to $I = A(1 - T/T_N)^{2\beta} + B$, with $T_N \approx 19.4$ K, $A = 3119$, $\beta = 0.23$ and $B = 1394$. The critical exponent β obtained corresponds to a 2D magnetic system, consistent with the layered structure of EuZn_2As_2 . Figure 3(d) shows the calculated structure factor square (F^2_{calc}) versus the observed one (F^2_{obs}). The linear behavior indicates excellent structure refinement. Any deviation is likely to be due to the errors resulting from the absorption correction process.

With an A-type magnetic structure (Figure. 3(b)), it is necessary to ask why both θ_{ab} and θ_c , obtained at temperatures well above T_N , are positive. For EuCd_2As_2 , both electron-spin resonance and muon-spin relaxation measurements reveal strong FM fluctuations with long time and length scales, which persist up to approximately 100 K [15]. Although this was not discussed in Ref. [15], we note that the electrical resistivity of EuCd_2As_2 also begins to show a negative slope below around 100 K. Bearing this in mind, we investigate the temperature and field dependence of both the ab -plane (ρ_{ab} , $I \parallel ab$) and c -axis (ρ_c , $I \parallel c$) resistivities. Figure 4(a) shows the temperature dependence of ρ_{ab} and ρ_c between 2 and 300 K for EuZn_2As_2 . Several features are worth mentioning. First, while $\rho_c > \rho_{ab}$ due to the layered structure of EuZn_2As_2 , ρ_{ab} and ρ_c show similar temperature dependence over the entire temperature range. This implies that the scattering mechanism is more or less the same in both the ab plane and the c direction. Similar behavior has also been reported for EuCd_2As_2 [26]. Second, there is a sharp peak in both ρ_{ab} and ρ_c , corresponding to the magnetic transition at T_N . The peak in ρ_c is even sharper than that in ρ_{ab} . Third, both ρ_{ab} and ρ_c initially vary linearly with temperature at high temperatures, deviating below $T_{fl} \approx 200$ K and eventually acquiring negative slopes ($d\rho_{ab}/dT < 0$ and $d\rho_c/dT < 0$) below ≈ 150 K. The sharp decrease of ρ_{ab} and ρ_c below T_N indicates that the resistivity in all directions is dominated by spin scattering above T_N . The departure from the high-temperature linear behavior marks the spin scattering contribution to the resistivity due to magnetic fluctuations below T_{fl} .

To confirm the effect of magnetic fluctuations on ρ_{ab} and ρ_c , the magnetic field dependence of ρ_{ab} and ρ_c at constant temperatures is investigated. Figure 4(b) and Figure 4(c) show the field dependence of the transverse ($H \perp I$) magnetoresistivity MR_{ab} ($I \parallel ab$, $H \parallel c$) and MR_c ($I \parallel c$, $H \parallel ab$) at various temperatures between 2 and 300 K, respectively. MR is defined by $\text{MR} = \frac{\rho(H) - \rho(H=0)}{\rho(H=0)} \times 100\%$. At 300 K, both MR_{ab} and MR_c are small and positive, typical for a paramagnetic material. Upon cooling, both MR_{ab} and MR_c gradually decrease and become negative near 200 K. With further cooling, their magnitudes continuously increase until T_N . The negative MR_{ab} and MR_c indicate the influence of ferromagnetic fluctuation below $T_{fl} \approx 200$ K, consistent with what is seen in EuCd_2As_2 [15]. Note that T_{fl} for EuZn_2As_2 is much higher than that in EuCd_2As_2 . Both higher T_{fl} and T_N offer wider temperature ranges for studying magnetism-related properties in EuZn_2As_2 than in EuCd_2As_2 .

At T_N , the spin scattering is almost completely suppressed, so that MR_{ab} and MR_c reach $\approx -90\%$ at $H > H_{sat}$. Below T_N , the field dependence of both MR_{ab} and MR_c is non-monotonic, with an initial increase followed by a decrease to negative values [Figures. 4(b) and 4(c)]. The initial positive MR_{ab} and MR_c is attributable to AFM interaction in both the ab plane and c direction (Figure 3(a))^[27]. With increasing field (less than 1 Tesla at 5 K), both MR_{ab} and MR_c start to decrease, eventually becoming negative and saturated above H_{sat} . This implies continuous alignment toward the ferromagnetic configuration. When H reaches H_{sat} , all moments are aligned ferromagnetically. Figure 4(d) shows the field dependence of MR_{ab} at various angles ϕ ($\phi = H \wedge I$ - defined in the inset) at $T = 0.6$ K. The low-field MR_{ab} peak is gradually suppressed as H turns away from the principal axes (ab - or c -axis). The inset of Figure 4(d) shows $MR_{ab}(\phi)$ at $\mu_0 H = 0.5$ and 6 T. Note that $MR_{ab}(\phi)$ reaches a minimum around $\phi = 45^\circ$, implying that there is field-induced spin reorientation pointing along the 45° direction between the ab -plane and c -axis.

With a strong magnetic fluctuation effect on the resistivity observed, it is interesting to consider the Hall response. Figure 4(e) shows the magnetic field dependence of the Hall resistivity (ρ_{xy}) at temperatures between T_N and 300 K. Surprisingly, ρ_{xy} increases linearly with magnetic field at all indicated temperatures, characteristic of the ordinary Hall effect. This means one can extract the Hall coefficient R_H via $\rho_{xy} = \mu_0 R_H H$ for each temperature. Figure 4(f) presents the temperature dependence of R_H , which increases with decreasing temperature. The positive R_H suggests that holes are dominant carriers in EuZn_2As_2 . Using the Drude relationship $R_H = 1/ne$, the carrier concentration n can be estimated. As shown in Figure 4(f), $n \approx 4 \times 10^{28} \text{ cm}^{-3}$ at room temperature, consistent with the semimetallic scenario for EuZn_2As_2 . It increases slightly with increasing temperature, which can be attributed to thermal effect if there is a small band gap as predicted in EuCd_2As_2 . Note that n becomes flat between approximately 100 K and T_{fl} , i.e., deviating from its behavior at both high- and low-temperatures. This suggests the influence of FM fluctuations to the band structure. It is our future work to elucidate the connection between magnetic fluctuations and possible topological phase transition in EuZn_2As_2 as discussed in EuCd_2As_2 ^[13-15].

4. Summary

We have successfully grown single crystalline EuZn_2As_2 , which forms a trigonal structure. The electrical resistivity, magnetization, and neutron diffraction investigation indicate that

EuZn₂As₂ orders antiferromagnetically below $T_N = 19$ K with an A-type spin configuration. Similar to EuCd₂As₂, there are strong FM fluctuations that give rise to profound spin scattering between T_N and $T_{fl} \approx 200$ K in EuZn₂As₂. Our MR_{ab} measurements with variable applied field direction indicate that there is field-induced reorientation of the spins to $\approx 45^\circ$ between the *ab*-plane and *c*-axis. Compared to EuCd₂As₂, the doubled T_N and T_{fl} make EuZn₂As₂ a better platform for exploring topological properties in both magnetic fluctuation ($T_N < T < T_{fl}$) and ordered ($T < T_N$) regimes. It is especially interesting to find out (1) if the reduced spin-orbit coupling in EuZn₂As₂ will reduce or close the gap between Dirac cones predicted in EuCd₂As₂, and (2) if the canted spin structure induced by magnetic field impacts the topological states.

5. Acknowledgements

Work at University of South Carolina and Louisiana State University is supported by NSF through Grant DMR-1504226. M.M. and W. X. were supported by the U.S. Department of Energy (DOE), Office of Science, Basic Energy Sciences under award DE-SC0022156. E.F. and H.B.C. are supported by the U.S. DOE, Office of Science, Office of Basic Energy Sciences, Early Career Research Program Award KC0402020, under Contract No. DE-AC05-e00OR22725. This research used resources at the High Flux Isotope Reactor and the Spallation Neutron Source, the DOE Office of Science User Facility operated by ORNL. A portion of this work was performed at the National High Magnetic Field Laboratory (NHMFL), which is supported by National Science Foundation Cooperative Agreement No. DMR- 1644779 and the Department of Energy (DOE). JS acknowledges support from the DOE BES program “Science at 100 T”, which permitted the design and construction of specialized equipment used in the high-field studies.

6. Conflict of interest

Authors declare no conflict of interests.

7. References

- [1] M. Z. Hasan, C. L. Kane, *Rev. Mod. Phys.* **2010**, *82*, 3045.
- [2] Z. K. Liu, J. Jiang, B. Zhou, Z. J. Wang, Y. Zhang, H. M. Weng, D. Prabhakaran, S.-K. Mo, H. Peng, P. Dudin, T. Kim, M. Hoesch, Z. Fang, X. Dai, Z. X. Shen, D. L. Feng, Z. Hussain, Y. L. Chen, *Nat. Mater.* **2014**, *13*, 677.
- [3] Z. K. Liu, B. Zhou, Y. Zhang, Z. J. Wang, H. M. Weng, D. Prabhakaran, S.-K. Mo, Z. X. Shen, Z. Fang, X. Dai, Z. Hussain, Y. L. Chen, *Science* **2014**, *343*, 864.
- [4] G. Zheng, J. Lu, X. Zhu, W. Ning, Y. Han, H. Zhang, J. Zhang, C. Xi, J. Yang, H. Du, K. Yang, Y. Zhang, M. Tian, *Phys. Rev. B* **2016**, *7*.
- [5] J. Jiang, Z. K. Liu, Y. Sun, H. F. Yang, C. R. Rajamathi, Y. P. Qi, L. X. Yang, C. Chen, H. Peng, C.-C. Hwang, S. Z. Sun, S.-K. Mo, I. Vobornik, J. Fujii, S. S. P. Parkin, C. Felser, B. H. Yan, Y. L. Chen, *Nat. Commun.* **2017**, *8*, 13973.
- [6] K. Deng, G. Wan, P. Deng, K. Zhang, S. Ding, E. Wang, M. Yan, H. Huang, H. Zhang, Z. Xu, J. Denlinger, A. Fedorov, H. Yang, W. Duan, H. Yao, Y. Wu, S. Fan, H. Zhang, X. Chen, S. Zhou, *Nat. Phys.* **2016**, *12*, 1105.
- [7] B. Q. Lv, H. M. Weng, B. B. Fu, X. P. Wang, H. Miao, J. Ma, P. Richard, X. C. Huang, L. X. Zhao, G. F. Chen, Z. Fang, X. Dai, T. Qian, H. Ding, *Phys. Rev. X* **2015**, *5*, 031013.
- [8] P. Li, Y. Wen, X. He, Q. Zhang, C. Xia, Z.-M. Yu, S. A. Yang, Z. Zhu, H. N. Alshareef, X.-X. Zhang, *Nat. Commun.* **2017**, *8*, 2150.
- [9] I. Belopolski, P. Yu, D. S. Sanchez, Y. Ishida, T.-R. Chang, S. S. Zhang, S.-Y. Xu, H. Zheng, G. Chang, G. Bian, H.-T. Jeng, T. Kondo, H. Lin, Z. Liu, S. Shin, M. Z. Hasan, *Nat. Commun.* **2017**, *8*, 942.
- [10] E. Emmanouilidou, H. Cao, P. Tang, X. Gui, C. Hu, B. Shen, J. Wu, S.-C. Zhang, W. Xie, N. Ni, *Phys. Rev. B* **2017**, *96*, 224405.
- [11] S.-G. Xu, Z.-J. Chen, X.-B. Chen, Y.-J. Zhao, H. Xu, X. Zhang, *Phys. Rev. B* **2020**, *102*, 125123.
- [12] G. Hua, S. Nie, Z. Song, R. Yu, G. Xu, K. Yao, *Phys. Rev. B* **2018**, *98*, 201116.
- [13] J. Ma, H. Wang, S. Nie, C. Yi, Y. Xu, H. Li, J. Jandke, W. Wulfhekkel, Y. Huang, D. West, P. Richard, A. Chikina, V. N. Strocov, J. Mesot, H. Weng, S. Zhang, Y. Shi, T. Qian, M. Shi, H. Ding, *Adv. Mater.* **2020**, *32*, 1907565.
- [14] M. C. Rahn, J.-R. Soh, S. Francoual, L. S. I. Veiga, J. Strempler, J. Mardegan, D. Y. Yan, Y. F. Guo, Y. G. Shi, A. T. Boothroyd, *Phys. Rev. B* **2018**, *97*, 214422.
- [15] J.-Z. Ma, S. M. Nie, C. J. Yi, J. Jandke, T. Shang, M. Y. Yao, M. Naamneh, L. Q. Yan, Y. Sun, A. Chikina, V. N. Strocov, M. Medarde, M. Song, Y.-M. Xiong, G. Xu, W. Wulfhekkel, J. Mesot, M. Reticcioli, C. Franchini, C. Mudry, M. Müller, Y. G. Shi, T. Qian, H. Ding, M. Shi, *Sci. Adv.* **2019**, *5*, eaaw4718.
- [16] G. M. Sheldrick, *Acta Crystallogr. Sect. C Struct. Chem.* **2015**, *71*, 3.
- [17] J. Rodríguez-Carvajal, *Phys. B Condens. Matter* **1993**, *192*, 55.
- [18] K. Momma, F. Izumi, *J. Appl. Crystallogr.* **2011**, *44*, 1272.
- [19] H. Cao, B. C. Chakoumakos, K. M. Andrews, Y. Wu, R. A. Riedel, J. Hodges, W. Zhou, R. Gregory, B. Haberl, J. Molaison, G. W. Lynn, *Crystals* **2019**, *9*, 5.
- [20] A. L. Spek, *J. Appl. Crystallogr.* **2003**, *36*, 7.
- [21] A. L. Spek, *Acta Crystallogr. Sect. C Struct. Chem.* **2015**, *71*, 9.
- [22] N. H. Jo, B. Kuthanazhi, Y. Wu, E. Timmons, T.-H. Kim, L. Zhou, L.-L. Wang, B. G. Ueland, A. Palasyuk, D. H. Ryan, R. J. McQueeney, K. Lee, B. Schrunck, A. A. Burkov, R. Prozorov, S. L. Bud'ko, A. Kaminski, P. C. Canfield, *Phys. Rev. B* **2020**, *101*, 140402.

- [23] J. Jensen, A. R. Mackintosh, *Rare Earth Magnetism*, Clarendon Press, Oxford, **1991**.
- [24] S. Pakhira, T. Heitmann, S. X. M. Riberolles, B. G. Ueland, R. J. McQueeney, D. C. Johnston, D. Vaknin, *ArXiv200906880 Cond-Mat* **2020**.
- [25] S. X. M. Riberolles, T. V. Trevisan, B. Kuthanazhi, T. W. Heitmann, F. Ye, D. C. Johnston, S. L. Bud'ko, D. H. Ryan, P. C. Canfield, A. Kreyssig, A. Vishwanath, R. J. McQueeney, L.-L. Wang, P. P. Orth, B. G. Ueland, *Nat. Commun.* **2021**, *12*, 999.
- [26] H. P. Wang, D. S. Wu, Y. G. Shi, N. L. Wang, *Phys. Rev. B* **2016**, *94*, 045112.
- [27] H. Yamada, S. Takada, *J. Phys. Soc. Jpn.* **1973**, *34*, 51.

Figure 1. (a) The crystal structure of EuZn_2As_2 . The pink, green and grey balls represent Eu, As and Zn atoms, respectively. (b) The PXRD pattern of EuZn_2As_2 single crystal. Inset: picture of EuZn_2As_2 single crystal.

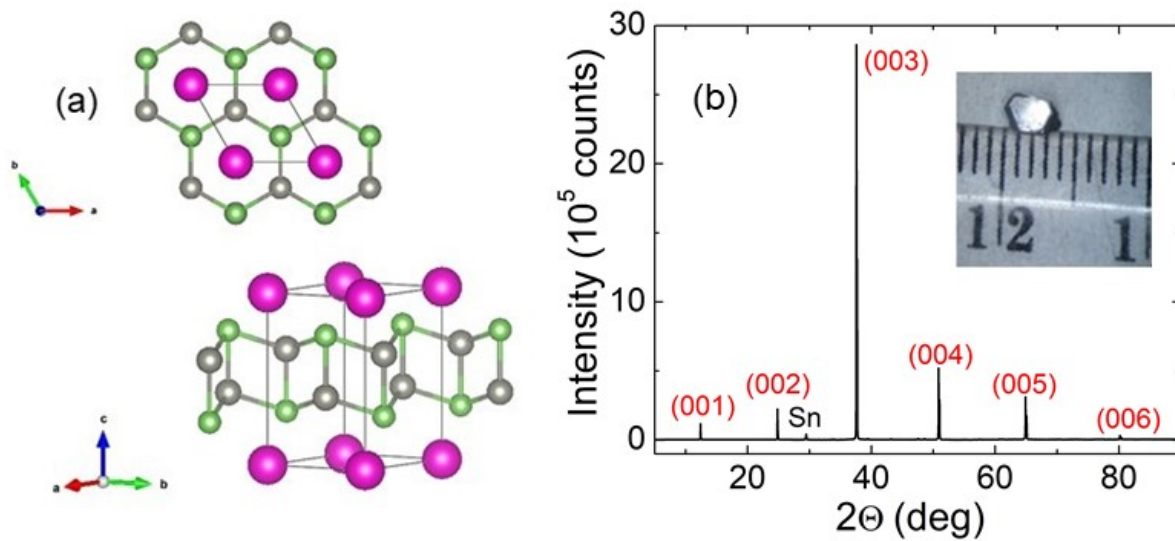


Figure 2. (a) The temperature dependence of the magnetic susceptibility measured along ab-plane (χ_{ab}) and c-axis (χ_c). Inset: the inverse magnetic susceptibility measured along ab-plane and c-axis with the Curie-Weiss fit discussed in the text. χ_{ab} and χ_c measured at several magnetic fields as a function of temperature (b) and (c), respectively. (d) $H - T$ phase diagram constructed using χ_{ab} and χ_c in Figure (b) and (c). (e) Magnetic hysteresis loop measured along ab-plane (χ_{ab}) and c-axis (χ_c). (f) The temperature dependence of specific heat. Inset: the specific heat measured with $H = 0$ T and 9 T.

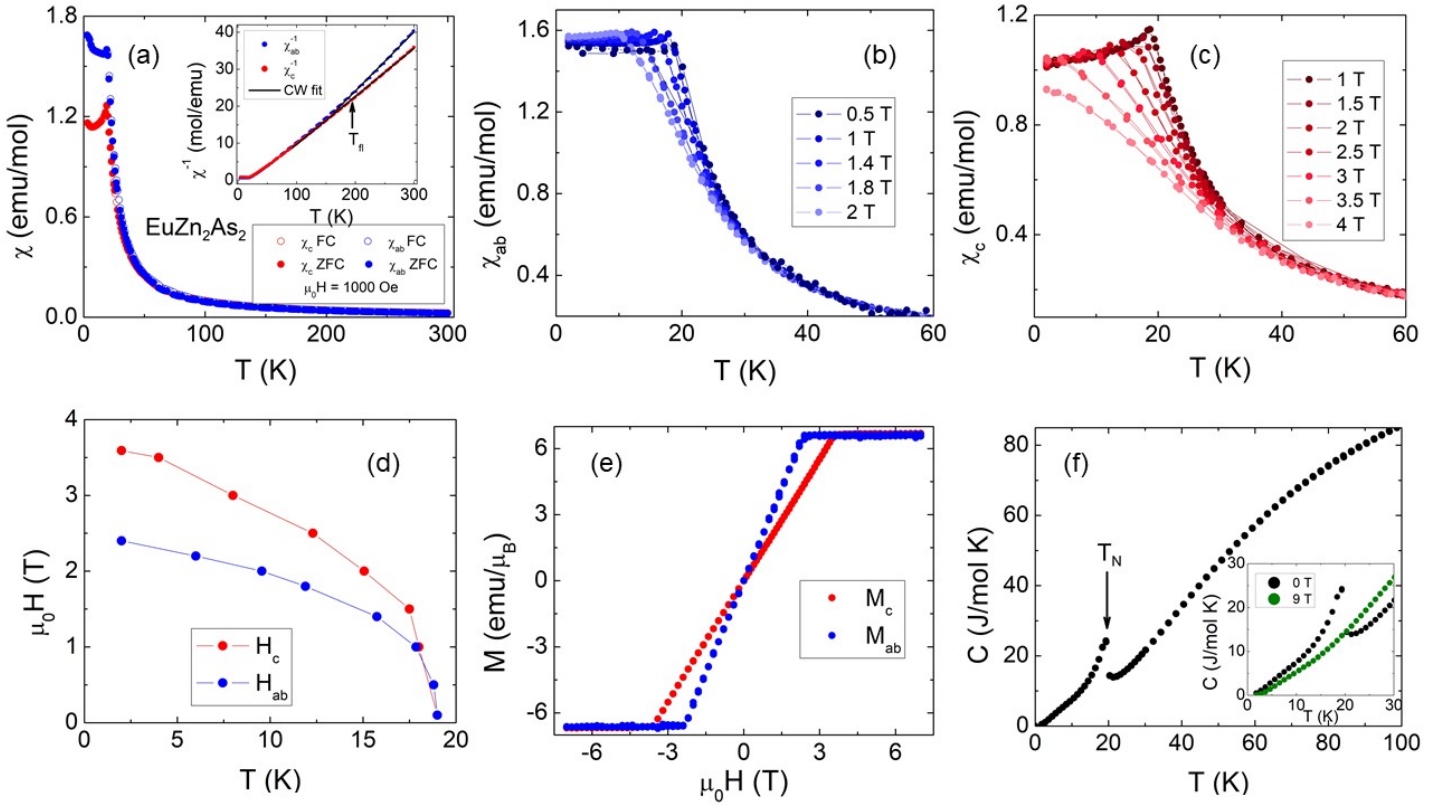


Figure 3. (a) The rocking curve scans at $(0\ 0\ \frac{1}{2})$ at 4 K and 40 K, measured by neutrons. (b) magnetic structure of Eu sublattice obtained at $T = 4$ K. (c) The peak intensity as a function of temperature with the empirical law fit (red solid line) discussed in the text. (d) Calculated structure factor square (F^2_{calc}) versus the observed one (F^2_{obs}).

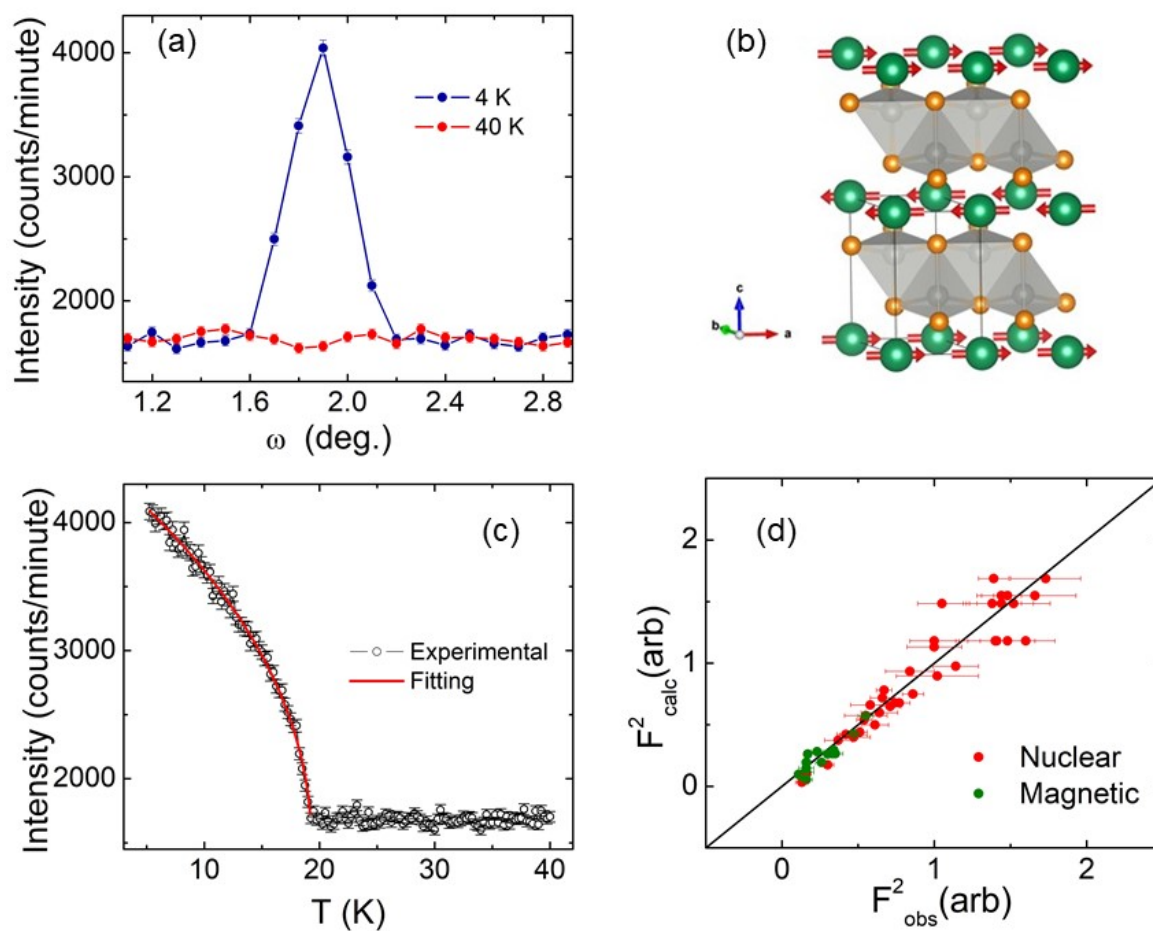


Figure 4. (a) Electrical resistivity as a function of temperature measured along ab-plane and c-axis. MR_{ab} (b) and MR_c (c) measured at several temperatures. (d) The magnetic field dependence of magnetoresistivity measured at several different angles. Inset: magnetoresistivity versus angle taken at magnetic field $\mu_0 H = 0.5$ T and 6 T. (e) Magnetic field dependence of Hall effect. (f) Hall coefficient and charge density as a function of temperature.

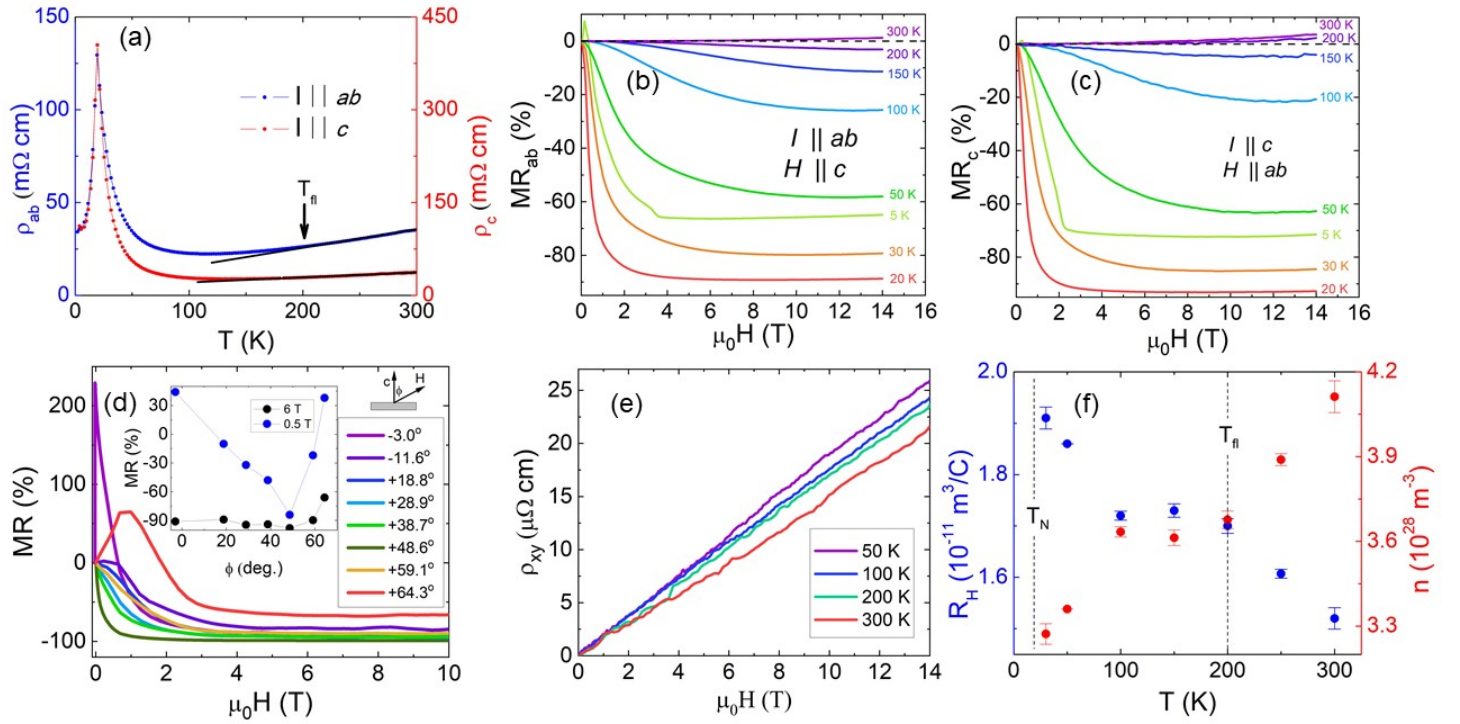


Table I. Single crystal crystallographic data and structure refinement for EuZn_2As_2 .

Formula	EuZn_2As_2
F. W. (g/mol)	432.54
Space group, Z	$P-3m1$ (#164),
a (Å)	4.2093(1)
b (Å)	4.2093(1)
c (Å)	7.175(3)
V (Å ³)	110.09(6)
Absorption correction	Numerical
Extinction coefficient	0.076(4)
Θ range (°)	2.839 - 33.143
hkl ranges	$-6 \leq h \leq 5$ $-6 \leq k \leq 6$ $-11 \leq l \leq 10$
No. reflections, R_{int}	1575, 0.0433
No. independent reflections	195
No. parameters	7
R_1, wR_2 (all I)	0.0258, 0.0378
Goodness of fit	1.084
Largest diff. peak and hole (e ⁻ /Å ³)	-1.477, 2.013

Table II. Atomic coordinates and isotropic displacement parameters of EuZn_2As_2 . U_{eq} is defined as one-third of the trace of the orthogonalized U_{ij} tensor (\AA^2).

Atom	Wyckoff	Occupancy	x	y	z	U_{eq}
Eu	1b	1	0	0	0	0.0083(2)
Zn	2d	1	1/3	2/3	0.2667(9)	0.0074(2)
As	2d	1	1/3	2/3	0.6296(3)	0.0106(2)